16th World Conference on Earthquake, 16WCEE 2017
Santiago Chile, January 9th to 13th 2017
Paper N° XXXX (Abstract ID)
Registration Code: S-XXXXXXXX

Factors Affecting Overturning of Buildings Induced by Tsunami Run-up in the 2011 Great Tohoku Earthquake

Michitaka Ishida[(1)], Kohji Tokimatsu[(2)], and Shusaku Inoue[(3)]

[(1)] *Graduate Student, Tokyo Institute of Technology, 1sh1da.to.be0@gmail.com*
[(2)] *Professor, Tokyo Institute of Technology, tokimatsu@arch.titech.ac.jp*
[(3)] *Associate Chief Researcher, Takenaka Corporation, inoue.shuusaku@takenaka.co.jp*

Abstract

Two- and three-dimensional tsunami run-up analyses were conducted to investigate the mechanisms and differences in overturning failures of five buildings (Building A to E) in Onagawa during the 2011 Great Tohoku earthquake. Several buildings including Buildings A and D overturned landward, while Building C with spread foundation overturned seaward and Building E overturned almost parallel with the coastline. A simple pseudo-static analysis using the hydrodynamic force and buoyant force estimated from the 2D analysis was able only to predict the overturning directions of Buildings A to D, suggesting Building E unlikely overturned due to the tsunami-induced hydrodynamic force and buoyant force alone. The 3D tsunami analysis has shown that the major cause of the overturning of Building E was the collision impact on this building of the drifting right section of Building D.

Keywords: Tsunami Load, Overturning Damage, Simulation of Tsunami Run-up, the 2011 Great Tohoku Earthquake

1. Introduction

The huge tsunami resulted from the 2011 Great Tohoku Earthquake (Mw 9.0) induced devastating damage to numerous structures along the east coast of Japan, claiming a death toll of over 15,000. The town of Onagawa, located on the coast in Miyagi Prefecture (Figure 1(a)), was one of the most heavily damaged areas, with an inundation depth of about 15m at the port area. The most remarkable feature in the town was several cases of overturned RC buildings by the tsunami in different forms. Sugimura et al. (2012) indicated several factors that may have caused overturning, such as hydrodynamic force, buoyant force, scour, liquefaction of underlying soil, and debris impact. However, it is not clear which factor or combination of factors was the main cause of overturning. Therefore, it is imperative to evaluate the cause of overturning to prevent occurrence of similar damage in future tsunamis.

This study investigates the factors having influenced damage to five buildings (Building A to E) in Onagawa. For this purpose, two- and three-dimensional (2D and 3D) analyses of the tsunami run-up as well as simple pseudo-static analysis using the hydrodynamic force and buoyant force estimated from the 2D analysis are performed.

2. Description of buildings investigated

Figure 1(b) shows a map of Onagawa town before the tsunami (after Geospatial Information Authority of Japan, GSI) with the locations of Buildings A to E investigated in this study. The figure also shows the area inundated by the tsunami during the 2011 Great Tohoku earthquake (Haraguchi and Iwamatsu, 2011), suggesting that most of the lower part of the town was damaged by the tsunami.

Figure 2(a) is a photograph taken during the first tsunami backwash from a hill at Site B shown in Figure 1, and Figure 2(b) is a photograph taken during the second tsunami run-up from a surviving building at Site C shown in Figure 1, suggesting that the overturning damage of the buildings had occurred likely during the first tsunami run-up that resulted in the maximum inundation depth. Figure 3 shows an enlarged map around Buildings A to E with their locations before and after the event as well as their overturning directions. Building A and D overturned landward whereas Building C overturned seaward, Building E overturned almost perpendicular to the coastline, and Building B did not overturn and remained at its original position.

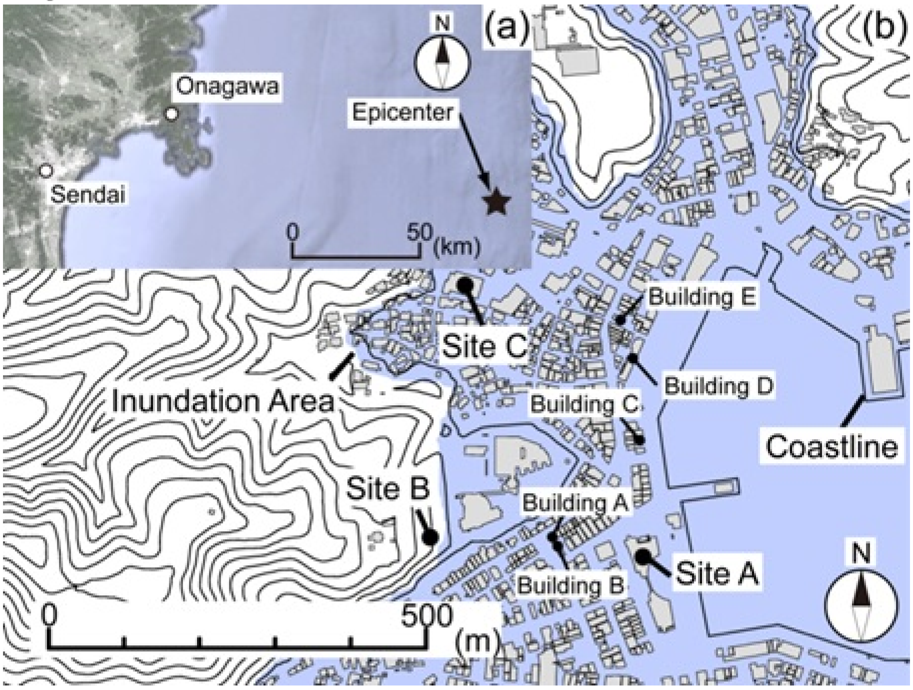

Fig. 1. Map of Onagawa and inundation area

Fig. 2. Tsunami run-up

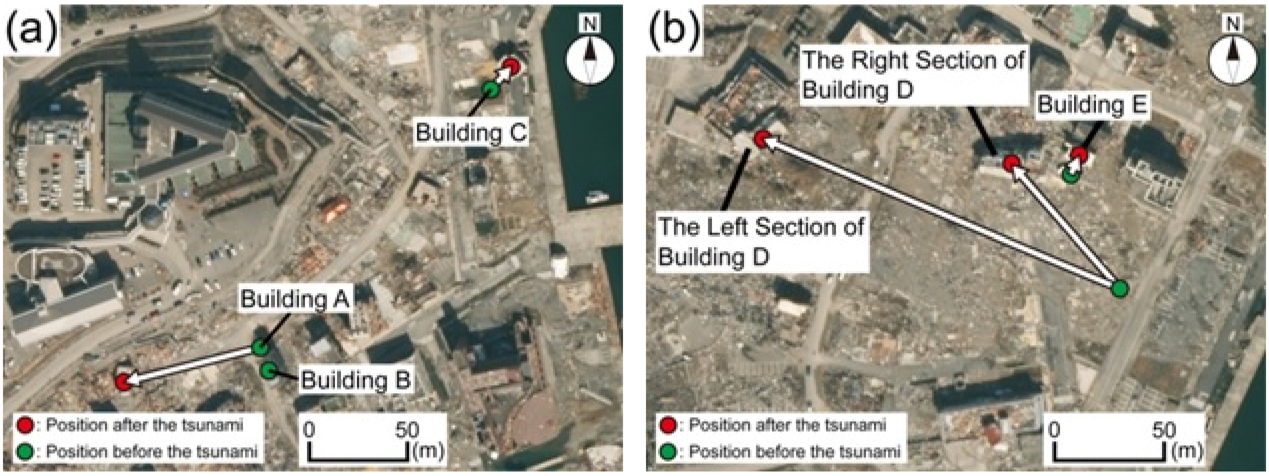

Fig. 3. Location and overturning direction of the five buildings investigated

Table 1 summarizes the general information of the buildings, in which *W* is the estimated weight, *H* is the height, *B* is the width in parallel to the coastline, L is the length perpendicular to the coastline, and D_f is the depth of foundation embedment.

Figure 4 shows Building A, a four-story RC building with pile foundation that overturned landward and displaced 70m from its original position. The pile foundation had 32 RC piles 4m long and 300mm in diameter, and all piles except one were broken at or near the pile head. One pile was pulled 3m up at its original position, and the exposed steel reinforcement had cut and thinning ends. This type of break is caused by tensile failure, which means that the piles were able to generate pull-out resistance.

Figure 5 shows Building B, a five-story RC building with pile foundation and did not overturn or displace. At this site, the ground subsidence indicates soil liquefaction (Tokimatsu et al., 2012). However, because the piles of the neighboring building A were able to generate pull-out resistance, the influence of liquefaction was not considered in the following analysis.

Figure 6 shows Building C, a four-story RC building with spread foundation that toppled and displaced 10m from its original position. This is the only building that overturned seaward. The fourth floor of the building detached and is missing

Table 1 – General information of buildings investigated

Building ID	W (MN)	H (m)	B (m)	L (m)	Df (m)
A	2.5	12.4	7.3	5.5	0.9
B	6.2	17.1	13.0	6.5	0.9
C	3.8	9.5	6.7	10.4	0.6
D	32.4	9.0	59.4	11.8	0.9
E	1.9	6.3	5.0	11.0	0.6

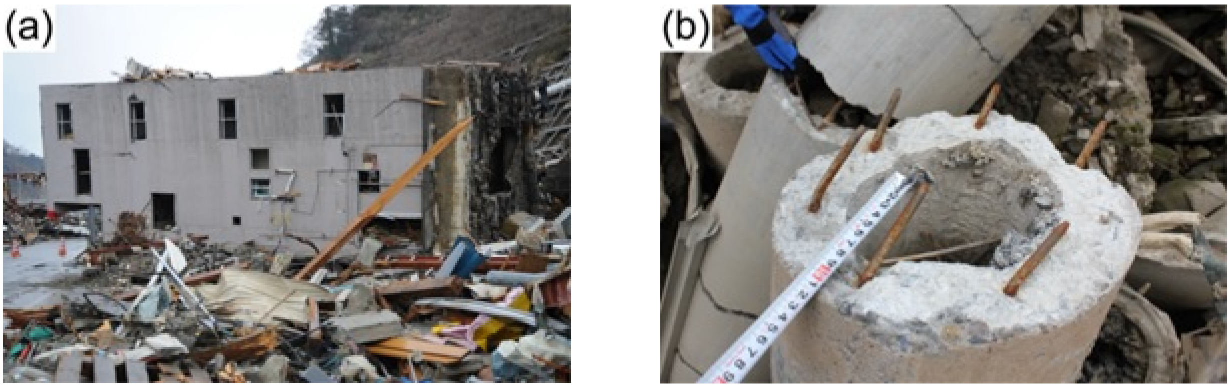

Fig. 4. Photos of Building A taken after the tsunami

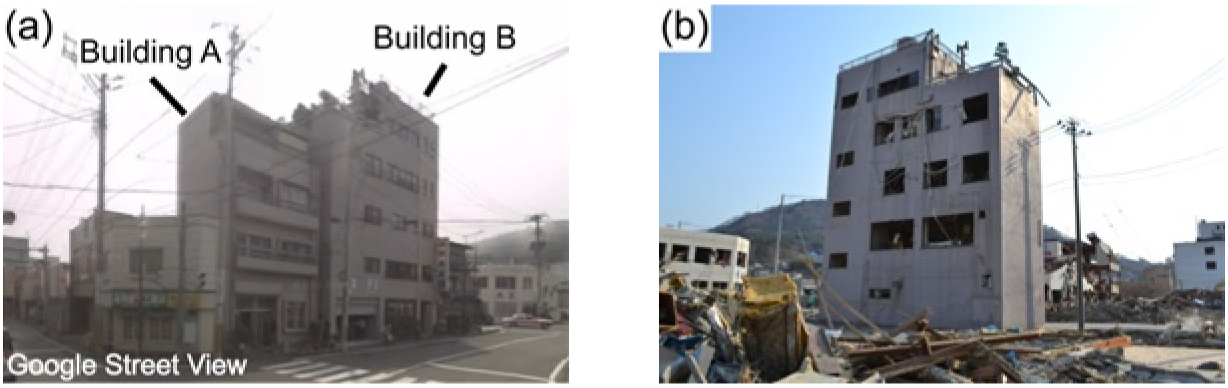

Fig. 5. Photos of Building B taken before and after the tsunami

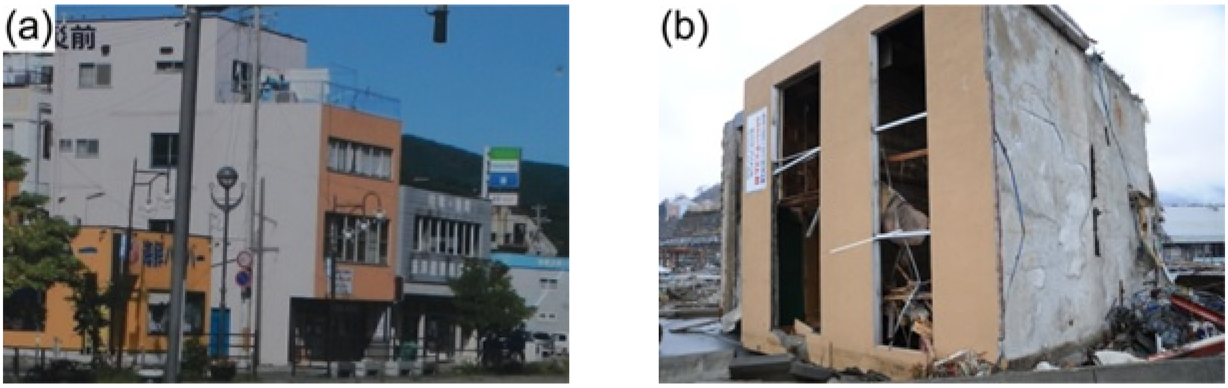

Fig. 6. Photos of Building C taken before and after the tsunami

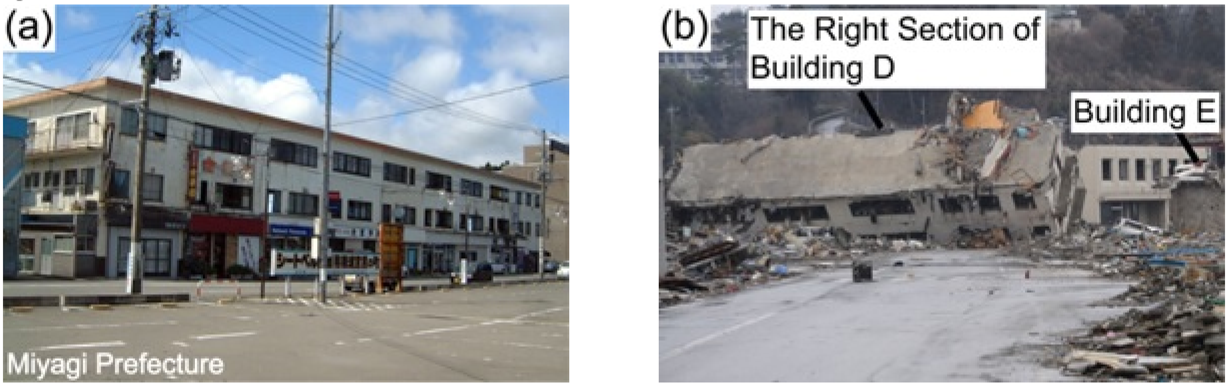

Fig. 7. Photos of Building D taken before and after the tsunami

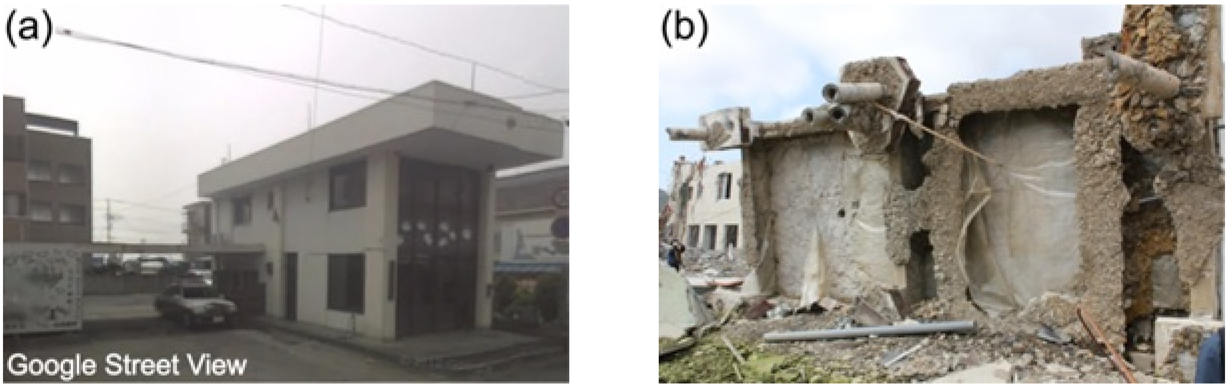

Fig. 8. Photos of Building E taken before and after the tsunami

Figure 7 shows Building D, a three-story RC building with spread foundation that overturned, split into three sections and drifted landward. While the middle section of this building was unidentified, the left section seen from the sea was found about 175 m landward from its original position and the right section about 75 m landward near Building E.

Figure 8 shows Building E, a two-story RC building with pile foundation that toppled in parallel to the shoreline at its original location. The pile foundation had 14 PC piles 20m long and 300mm in diameter (NILIM, 2012), and failed at the pile head or 0.9m to1.5m below the pile head, suggesting a tensile failure of pile. This indicates that the tensile strength of the pile was likely less than the pull-out resistance of the pile.

3. Evaluation of damage of Building A to C

3.1 2D simulation of the tsunami run-up

A 2D analysis of the tsunami run-up was conducted with a shallow water theory (Hirt and Richardson, 1999). The 2D area demarcated with red lines in Figure 9 is the concerned area for 2D analysis, which has a dimension of 1530m and 570m with uniform mesh of 10m by 10m. The terrain model using the 2D analysis was assigned according to the digital elevation model (DEM) provided by the GSI and General Ground Plan of Onagawa Port, Miyagi, available from Japan Center for Asian Historical Records (JACAR).

The open circles and solid black lines in Figure 10 are the inundation depth and flow velocity around Site A shown in Figure 1 evaluated from the video analysis of the first tsunami run-up (Koshimura et al., 2012). The blue line shown in Figure 10(a) is the smoothed inundation depth, which plus the elevation of Site A was used as the time history of the sea water level assumed at the seaside (east) boundary of the analysis area. The red lines in Figure 10(a) and (b) show the computed inundation depth and flow velocity (red lines) at Site A. The computed inundation depth at Site A corresponds reasonably well to one estimated from the video analysis. The computed flow velocity also corresponds reasonably well to the observed one, except the early stage of the tsunami run-up. Figure 11 shows the distribution of the inundation depth and flow velocity computed by the analysis. The inundation area shown in Figure 11 by the analysis corresponds well to the observed one.

Fig. 9. Analyzed area for the 2D simulation

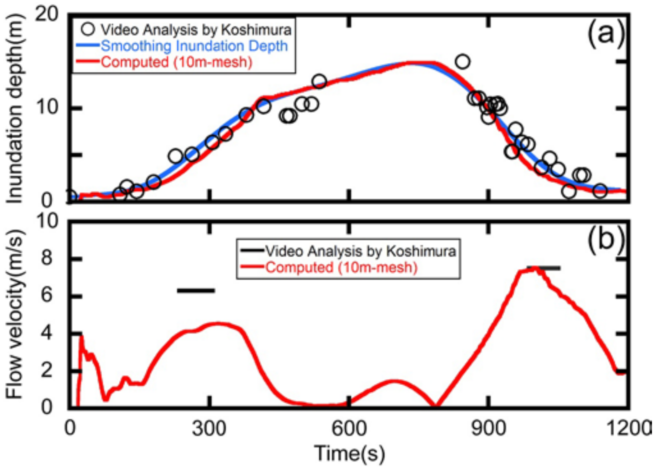

Fig. 10. Inundation depth and flow velocity

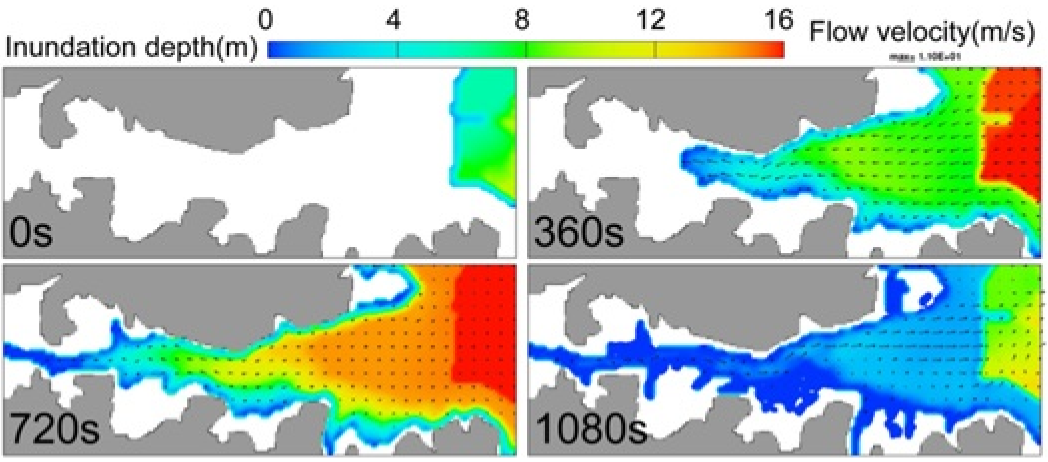

Fig. 11. Distribution of inundation depth and flow velocity

3.2 Method for estimating tsunami-induced damage to buildings

Figure 12 shows simplified free body diagrams for sliding, uplift, and overturning mechanisms. In the sliding model, we assumed that the resisting forces against hydrodynamic force were the shear strength of the rebar of piles and the passive earth pressure acting the embedded foundation for a building with pile foundation and the base friction and passive earth pressure for a building with spread foundation. In the uplift model, the resisting force against buoyant force was the pull-out resistance for a building with pile foundation and the self-weight for a building with spread foundation. In the overturning model, the resisting forces acting against overturning moment induced by hydrodynamic force and buoyant force with respect to the rotation center shown in Figure 12(c) were the pull-out resistance and the self-weight for a building with pile foundation and the self-weight for a building with spread foundation. The pull-out resistance was likely either the piles skin friction or the tensile strength of the rebar of piles whichever is smaller.

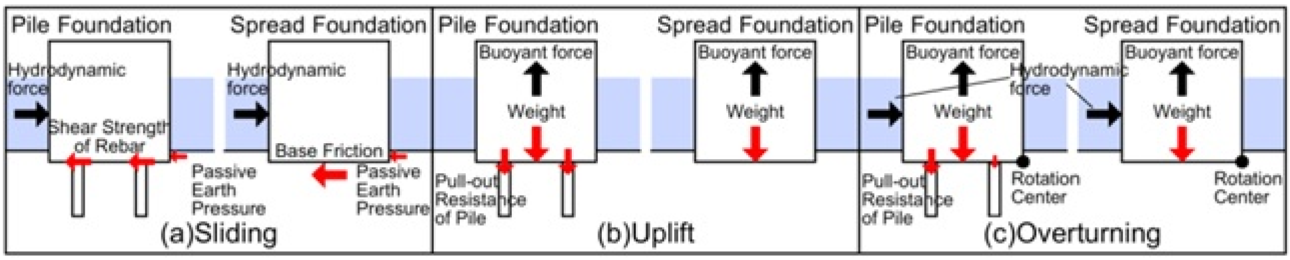

Fig. 12. Evaluation model of sliding, uplift, and overturning

The hydrodynamic force F_D acting on a building in the travel direction of tsunami may be calculated by the following formula (FEMA, 2012);

$$F_D(t) = \frac{1}{2}\rho C_D u(t)^2 h(t) B \tag{1}$$

where ρ is the fluid density including sediment (1.2t/m^3), C_D is the drag coefficient (2.0), u and h are the flow velocity and inundation depth computed by the 2D simulation.

The buoyant force F_B acting on the building is calculated by the following formula;

$$F_B(t) = \rho g \left\{ V(t) - V_W(t) \right\} \tag{2}$$

where g is gravitational acceleration (9.8m/s^2), V is the volume of the building below the inundation depth, and V_W is the volume of water entering the building.

The flow rate of the water entering the building, $\Delta V_W(t)$, during the tsunami run-up was estimated by multiplying the area of the building openings between the interior and exterior inundation depths, *As(t)*, by the current flow velocity, *u(t)*. The height to be filled by water in each floor was limited by either the inundation depth or the highest height of the opening of the floor that creates dead air space above, whichever is lower. $V_W(t)$ during the backwash was assumed to be equal to the volume inside the building below the inundation depth, *h(t)*, regardless of the current flow velocity, *u(t)*, and the presence of dead air space during run-up. The value of V_W was also constrained by assuming that the dimension of pillar cross-section was 500mm × 500mm and the wall thickness was 200mm.

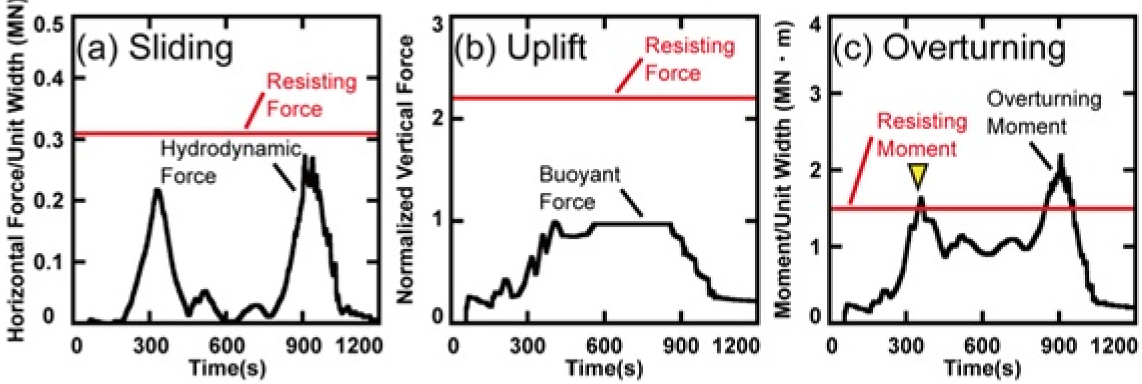

Fig. 13. Result of Building A for sliding, uplift, and overturning

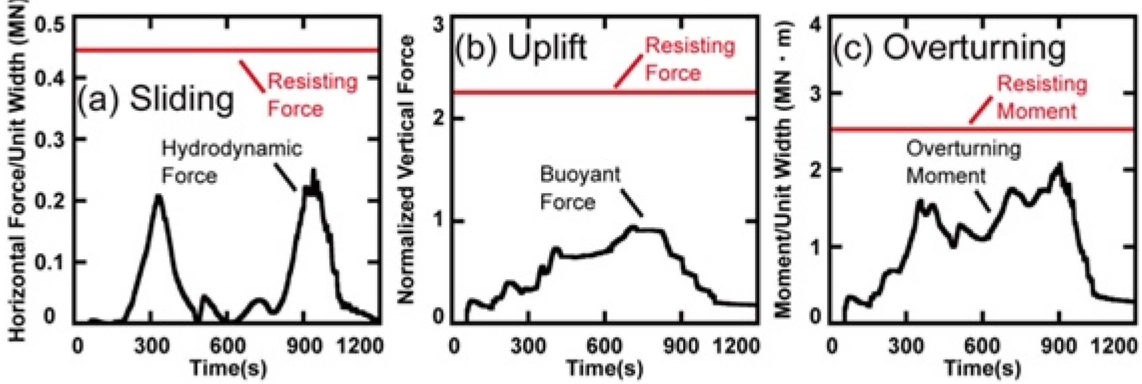

Fig. 14. Result of Building B for sliding, uplift, and overturning

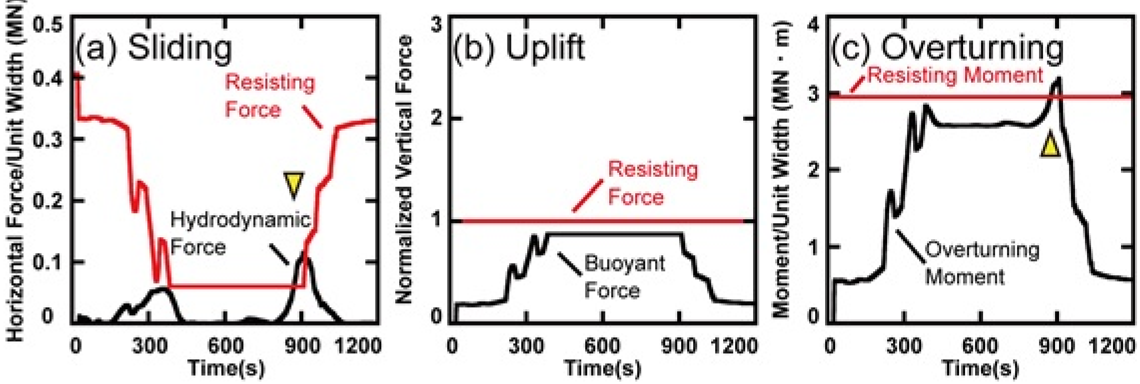

Fig. 15. Result of Building C for sliding, uplift, and overturning

Figures 13-15 show the time history of the driving forces/moment (black lines) and resisting forces/moment (red lines) for sliding, uplift, and overturning for Buildings A to C, computed from the simplified method. Figure 13 suggests that Building A failed due to overturning during the tsunami run-up, which corresponds with the field performance of this building that overturned landward. Figure 14 suggests that Building B did not overturn during the tsunami, which corresponds with the field performance of this building that did not overturn. Figure 15 suggests that Building C failed due to sliding and overturning during the tsunami backwash, which also corresponds with the field performance of this building that overturned seaward.

4. Evaluation of damage of Building D and E

4.1 Evaluation of building damage by the 2D simulation

For Building D and E, the simple pseudo-static analysis using the hydrodynamic force and buoyant force estimated from the 2D analysis was also performed. The 2D area demarcated with red lines in Figure 16(a) is the concerned area for 2D analysis, which has a dimension of 2960m and 3660m with uniform mesh of 10m by 10m. The terrain model using the 2D analysis was assigned according to the previous one. The blue line shown in Figure 17(a) is the time history of the sea water level assumed at the seaside (southeast) boundary of the analysis area.

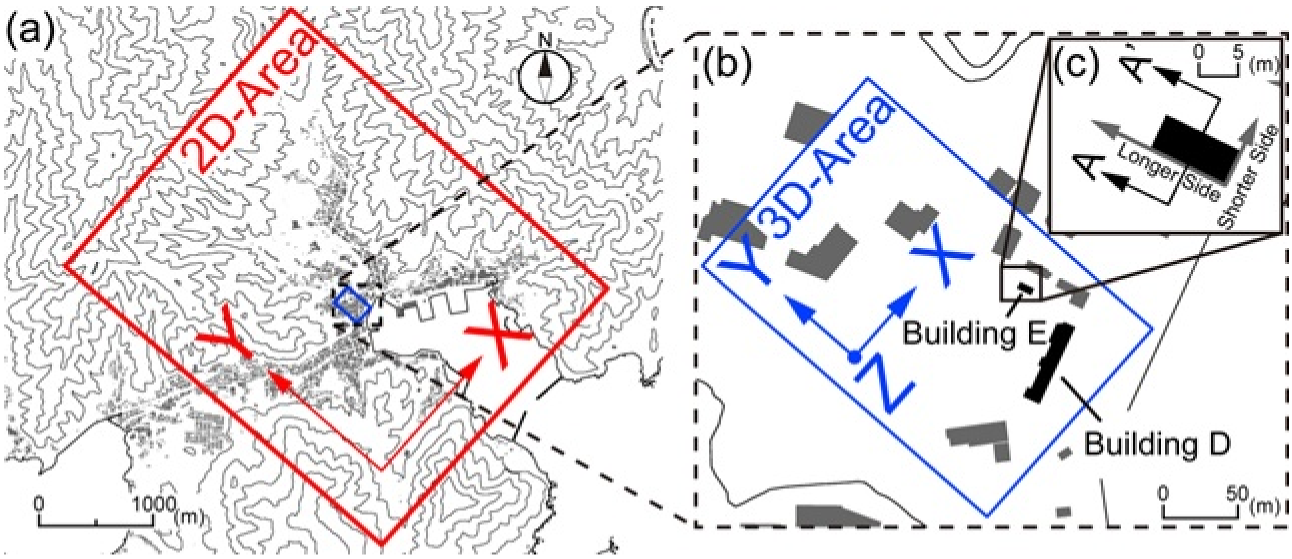

Fig. 16. Analyzed area for the 2D and 3D simulation

Figures 18-19 show the time history of the driving forces/moment (black lines) and resisting forces/moment (red lines) for sliding, uplift, and overturning for Buildings D and E, computed from the simplified method. Figure 18 suggests that Building D failed due to sliding and overturning during the tsunami run-up, which corresponds with the field performance of this building that overturned and drifted landward. Figure 19 suggests, in contrast, that Building E did not overturn during the tsunami, which contradicts the observed performance of this building that overturned. Moreover, the travel direction of tsunami at this site was the longer side direction of this building, which is inconsistent with the overturning direction of this building, i.e., the shorter side direction that was parallel with the coastline. This inconsistency motivated us to examine further the effects of 3D tsunami propagation as well as other possible factors not considered in 2D analysis.

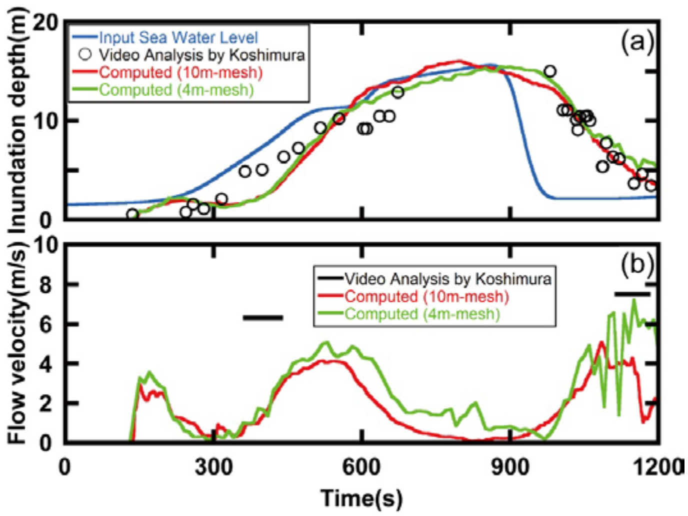

Fig. 17. Computed time histories of inundation depth and 2D flow velocity

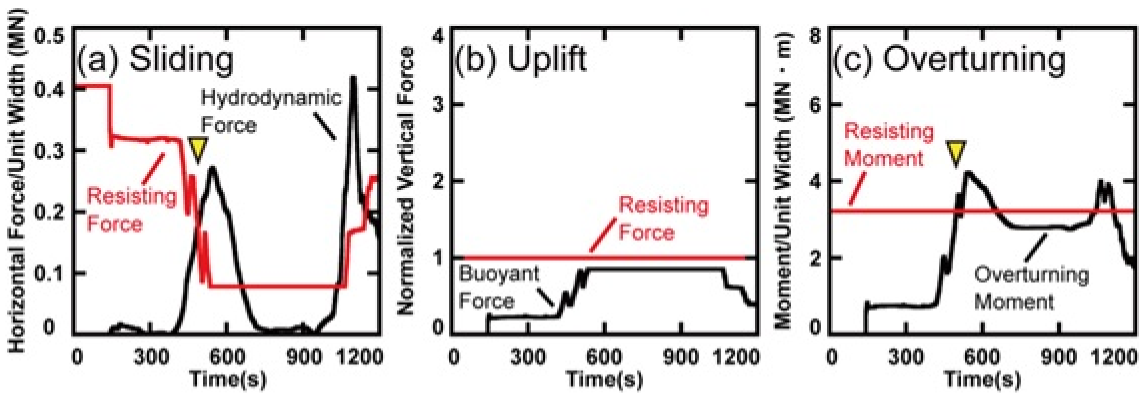

Fig. 18. Result of Building D for sliding, uplift, and overturning

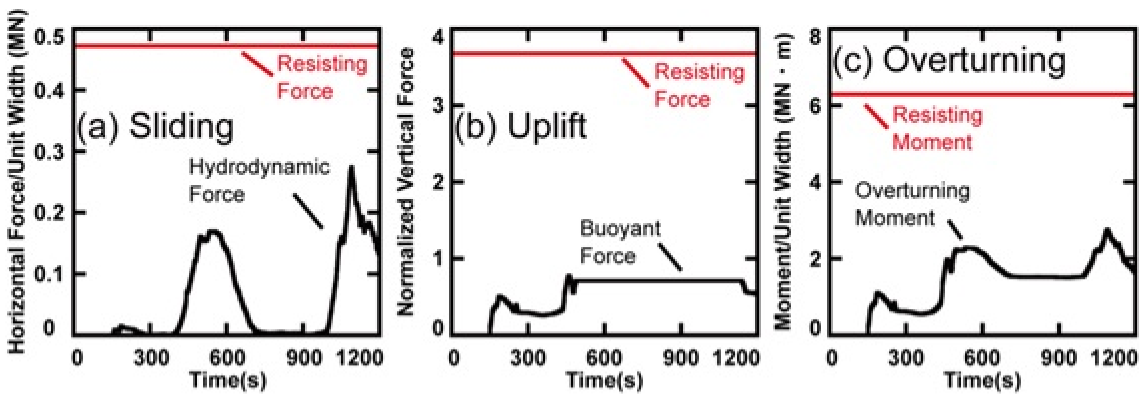

Fig. 19. Result of Building E for sliding, uplift, and overturning (2D)

4.2 3D simulation of the tsunami run-up

A 3D simulation of the tsunami run-up was conducted with Volume of Fluid (VOF) method (Hirt and Richardson, 1981) for the tsunami run-up phase only (until 970s). The area demarcated with blue lines shown in Figure 16(b) is the concerned area for the 3D analysis, which has a dimension of 176m and 270m and T.P. +50m to -29m with uniform mesh of 1m by 1m. The terrain model using the 3D simulation was one used for the 2D analysis plus the elevation of all surviving buildings in the area as well as Buildings D and E. The input boundary conditions assigned to the seaside of the 3D area were the inundation depth and flow velocity computed from the same 2D analysis described in the previous section. It was, however, conducted with more precise mesh of 4m by 4 m adding the elevation of the surviving buildings as well as Buildings D and E. In the 3D simulation of the tsunami run-up, Building D was divided along its longitudinal direction into three sections that can drift separately. The density of each section was assumed to be 1.09 t/m^3, which corresponds to the condition where the volume of water in the building is a half of the inside volume of the building. The coefficient of friction of the terrain model with respect to each drifting section was assumed to be 0.4.

Figure 17 also shows the inundation depth and flow velocity (green lines) at Site A computed from the 2D analysis with 4m meshes. The computed inundation depth and flow velocity are consistent with those estimated from the video analysis better than those computed with 10m meshes (red lines).

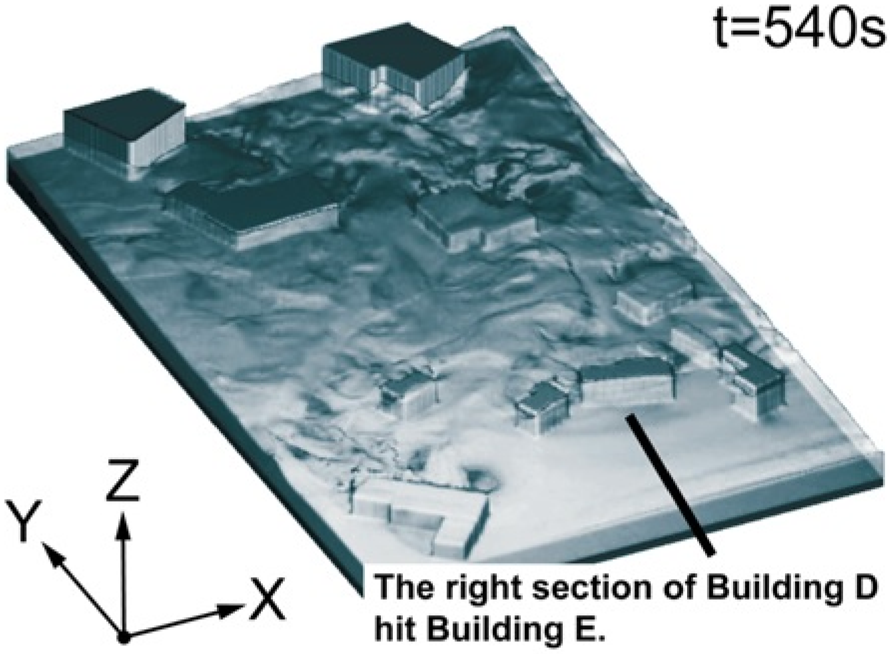

Fig. 20. Computed floating behavior of Building D at t=540s

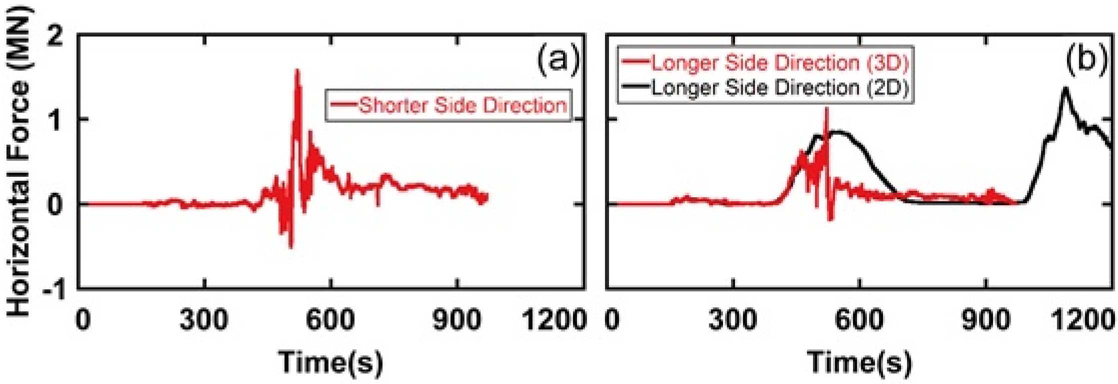

Fig. 21. Computed time histories of hydrodynamic force acting on Building E

Figure 20 shows the drifting behavior of Building D at 540s. The rightmost section of Building D hit Building E at this instance. This is consistent with the actual field observation such as shown in Figure 7(b), suggesting that the overturning of Building E in parallel to the coastline might have occurred due to the collision of the right section of Building D with Building E.

Figure 21 shows the computed time histories of hydrodynamic force (red lines) acting in the shorter and longer side directions of Building E computed by the 3D simulation. The figure also shows the calculated time histories of hydrodynamic force (black lines) acting in the longer side direction of Building E by the 2D simulation. A comparison of Figures 21(a) and (b) suggests that the peak horizontal force at the time of the collision is larger in the shorter side direction than in the longer side direction.

4.3 Evaluation of building damage by the 3D simulation

The simple pseudo-static analysis shown in Figure 12 was performed for Building E along its shorter side direction using the hydrodynamic and buoyant forces computed from the 3D and 2D analysis, respectively. Figure 22 shows the estimated loads (black lines) and resistances (red lines) for sliding, uplift, and overturning for Building E. The figure suggests that, without considering the effects of collision impact, Building E have not overturned during tsunami run-up.

The impact force of the drifting right section of Building D to Building E in its shorter side direction was not computed directly from the 3D analysis but estimated to be approximately 16MN, which is much greater than one inducing overturning of building, i.e., about 2MN. This suggests that the collision of a part of Building D is the major factor inducing the overturning of Building E in parallel to the coastline.

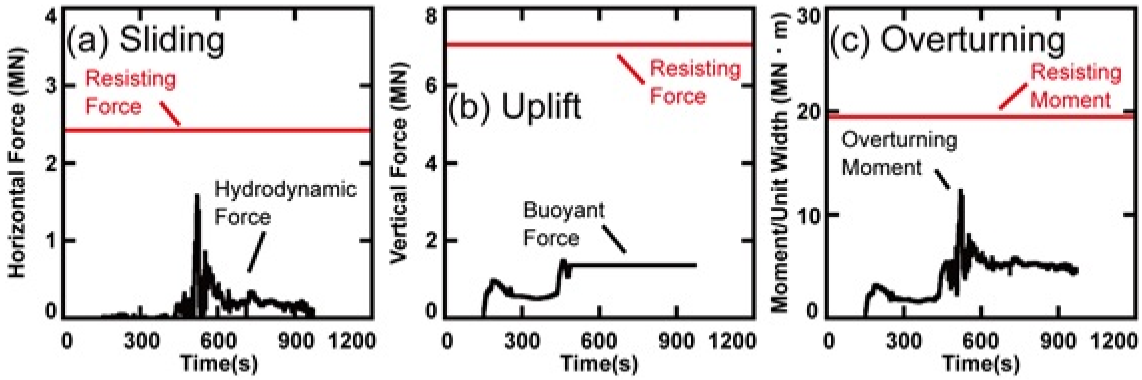

Fig. 22. Result of Building E for sliding, uplift, and overturning (3D)

5. Conclusions

Two- and three-dimensional tsunami simulation analyses were conducted to investigate the major factors inducing the difference in damage among five buildings (Building A to E). A simple pseudo-static analysis using the hydrodynamic force and buoyant force estimated from the 2D analysis was able to predict the field performance of Buildings A to D, but suggesting that Building E unlikely overturned due to the tsunami-induced hydrodynamic force and buoyant force alone. The 3D tsunami analysis has shown that the major cause of the overturning of Building E was the collision impact on this building of the drifting right section of Building D.

6. Acknowledgements

Several photographs used in the paper were credited to Yahoo, East Japan Earthquake Project and Miyagi Prefecture, and Great East Japan Earthquake Archive Miyagi. Their permission for reuse of their photos is gratefully acknowledged.

7. References

[1] Sugimura, Y. and Mitsuji, K. (2012): The survey of buildings overturned and carried out by tsunami. *Foundation Engineering and Equipment*, Vol. 40, No.12, pp.71-75 (in Japanese).

[2] Haraguchi, T. and Iwamatsu, A. (2011): *Detailed Maps of the Impacts of the 2011 Japan Tsunami Vol.1: Aomori, Iwate and Miyagi prefectures*, Kokon-Shoin Publishers, 167pp.

[3] Yahoo, *East Japan Earthquake Picture Project*, available at http://archive.shinsai.yahoo.co.jp/ (last accessed 23 February, 2016)

[4] Miyagi Prefecture, *Great East Japan Earthquake Archive Miyagi - Onagawa Town*, available at http://kioku.library.pref.miyagi.jp/onagawa/ (last accessed 23 February, 2016)

[5] Geospatial Information Authority of Japan (GSI), available at

http://mapps.gsi.go.jp (last accessed 23 February, 2016)

[6] Google, *Memories for the Future*, available at http://www.miraikioku.com/ (last accessed 23 February, 2016)

[7] Tokimatsu, K., Tamura, S., Suzuki, H. and Katsumata, K. (2012): Buildings damage associated with geotechnical problems in the 2011 Tohoku Pacific Earthquake. *Soil and Foundation*, Vol. 52, No.5, pp.956-974

[8] National Institute for Land and Infrastructure Management, Ministory of Land, Infrastructure and Transport, Japan (2012): Damage investigation report of the 2011 Tohoku-Pacific Ocean Earthquake, *TECHNICAL NOTE of NILIM*, No.674, 565pp. (in Japanese).

[9] Hirt, C.W. and Richardson, J.E. (1999): The modeling of shallow flows. *Flow Science, Inc., Technical Notes*, FSI-99-TN48R

[10] Japan Center for Asian Historian Records (JACAR). *Attachment, Onagawa Port, Miyagi, general ground plan*, Ref.A11112289000, Relevant Documents regarding Cabinet Tohoku Bureau, File of petition documents (two), 1935 (National Archives of Japan), available at http://www.digital.archives.go.jp/ (last accessed 23 February, 2016)

[11] Koshimura, S. and Hayashi, S. (2012): Tsunami flow measurement using the video recorded during the 2011 Tohoku tsunami attack. *International Geoscience and Remote Sensing Symposium*, IEEE international, pp.6693-6696

[12] Federal Emergency Management Agency (2008): Guideline for Design of Structures for Vertical Evacuation from Tsunamis. *FEMA P646*

[13] Hirt, C.W. and Nicholas, B.D. (1981): Volume of Fluid (VOF) Method for the Dynamics of Free Boundaries. *Jornal of Computational Physics*, 39, pp.201-225